

Orthonormal Product Quantization Network for Scalable Face Image Retrieval

Ming Zhang^{1,2*}, Xuefei Zhe³ and Hong Yan^{1,2}

¹Department of Electrical Engineering, City University of Hong Kong, Hong Kong, China.

²Centre for Intelligent Multidimensional Data Analysis Limited, Hong Kong, China.

³Tencent AI Lab, Shenzhen, China.

*Corresponding author(s). E-mail(s): ming@innocimda.com;
Contributing authors: elizhe@tencent.com; h.yan@cityu.edu.hk;

Abstract

Existing deep quantization methods provided an efficient solution for large-scale image retrieval. However, the significant intra-class variations like pose, illumination, and expressions in face images, still pose a challenge for face image retrieval. In light of this, face image retrieval requires sufficiently powerful learning metrics, which are absent in current deep quantization works. Moreover, to tackle the growing unseen identities in the query stage, face image retrieval drives more demands regarding model generalization and system scalability than general image retrieval tasks. This paper integrates product quantization with orthonormal constraints into an end-to-end deep learning framework to effectively retrieve face images. Specifically, a novel scheme that uses predefined orthonormal vectors as codewords is proposed to enhance the quantization informativeness and reduce codewords' redundancy. A tailored loss function maximizes discriminability among identities in each quantization subspace for both the quantized and original features. An entropy-based regularization term is imposed to reduce the quantization error. Experiments are conducted on four commonly-used face datasets under both seen and unseen identities retrieval settings. Our method outperforms all the compared deep hashing/quantization state-of-the-arts under both settings. Results validate the effectiveness of the proposed orthonormal codewords in improving models' standard retrieval performance and generalization ability. Combing with further experiments on two general image datasets, it demonstrates the broad superiority of our method for scalable image retrieval. The source codes will be released at <https://github.com/mzhang367/opqn> once the paper is accepted.

Keywords: Product quantization, Face image retrieval, Convolutional neural networks, Orthonormal codewords

1 Introduction

Rapid growth in the internet user population and the popularity of mobile devices with advanced

cameras have prompted the sharing of visual content on social media. A large number of user-generated human face images, e.g., selfies and

portraits, are uploaded every day. Due to the need for image indexing and searching, large-scale image retrieval has been an active area of research. Face image retrieval aims to return images from the database images that are of the same person as the query image. However, large intra-class variances caused by expressions, illumination, or occlusion, and small inter-class distances between visually similar people, make developing an accurate and efficient system for unconstrained face image retrieval challenging. Another problem is, in a real-world application where the number of newly joined identities keeps growing, high scalability of the retrieval system is needed. The poor generalization performance prevents scaling of these retrieval systems to larger datasets.

One basic idea for highly efficient image retrieval is using binary code representations to encode the data, thereby enabling an approximate nearest neighbor (ANN) search to accelerate the query process. According to their applied retrieval metrics, the works of obtaining binary code representations can be divided into two types: 1) Hamming distance- or 2) dictionary-related distance-based. Following practice in the literature (Klein and Wolf, 2019; Jang and Cho, 2020; Yu et al, 2020), we refer to Hamming distance-based approaches as *hashing* models and dictionary-related distance-based approaches as *quantization* models. The goal of hashing is to map high dimensional real-valued data to lower

dimensional binary codes in Hamming space while preserving their original similarity. The Hamming distance of the binary codes between the query and database images can be computed extremely fast by the XOR operation. By exploiting semantic labels to learn the hashing function, supervised hashing (Shen et al, 2015; Gui et al, 2017) usually outperforms unsupervised hashing (Weiss et al, 2009; Gong et al, 2012) with better semantic similarity measurements. Recently, supervised deep hashing (Li et al, 2016; Lin et al, 2017; Yuan et al, 2020), using deep convolutional neural networks (CNNs), was proposed for end-to-end learning of feature representations and hashing functions and substantially outperformed traditional hashing methods for image retrieval.

For any pair of binary codes of length l , hashing-based methods can only generate $l + 1$ distinct values to depict their pairwise similarity making it hard to draw rich similarity relations for large-scale face image datasets with many classes of identities. Another disadvantage is most hashing methods obtain binary codes by applying a sign function to continuous features (Li et al, 2017; Lin et al, 2017; Zhang and Yan, 2021). To solve the intractable discrete optimization in the training process, they usually relax the discrete constraint to be continuous and convert it to a regularization term. Consequently, it causes inevitable information loss.

In parallel with binary hashing, product quantization (PQ) (Jegou et al, 2010; Ge et al, 2013; Zhang et al, 2014) has been widely employed in the fields of computer vision and information retrieval. It decomposes feature vectors in the original space into several disjoint sub-vectors. Each sub-vector then needs to find the nearest centroid (codeword) in the subspace (codebook). By replacing each sub-vector with the index of the nearest codeword, the original features in one subspace are encoded into binary codes. For binary codes of length $l = M \log_2 K$, where M is the number of codebooks, and K is the number of codewords in each codebook, PQ is capable of producing $\binom{K}{2}^M$ distinct distance values. Thus, it is more powerful to describe the similarity distance between fine-grained face samples. During the query stage, PQ-based methods allow the use of multiple lookup tables (LUTs) for query speed acceleration, which is only slightly more costly than hashing-based methods (Jegou et al, 2010; Cao et al, 2016). Although deep hashing has drawn increasing attention for face image retrieval (Tang et al, 2018; Xiong et al, 2020; Zhang et al, 2021), deep quantization methods are rarely publicly explored for the task.

The PQ technique was initially designed under the unsupervised setting. For example, the codewords in PQ could be iteratively updated by k -means clustering (Hartigan and Wong, 1979) on the sub-vectors in each subspace. Recently,

some deep quantization methods (Yu et al, 2018; Klein and Wolf, 2019) have been proposed to learn codewords with supervision. The feature representations are divided into several sub-vectors and quantized by learnable codewords depending on the similarity between the sub-vectors and codewords. Typically, a softmax or triplet loss can be constructed based on the resulting quantizations. Thereby, the learning metrics preserve the label information in both the feature representations and the learnable codewords. We refer to these deep quantization methods with the learning manner as *learning to quantization (l2q)*. However, since the codewords themselves do not contain any discriminative information for the quantization process, it is possible to decorrelate the discriminative visual information and codewords individually. Under this hypothesis, we can learn the codewords assignment of features representations even with predefined codewords. As described in Sect. 3.1, this is achieved by introducing one layer of parameters for quantization compositions in our method.

From the view of codewords, how codewords' distribution has an influence on the quantization quality is seldom explored previously. Intuitively, codewords in a codebook can be considered as prototypes in a subspace that spread over the subspace but should retain some distance from each other. To visualize how codewords are distributed in l2q methods, the angles between codeword pairs

in each codebook in two deep quantization models (Klein and Wolf, 2019; Jang and Cho, 2020) are calculated. Their distributions are illustrated in Figure 1(a) and (b). We can see that the compared methods show variable angular distributions, which are sub-optimal in terms of distinct codewords separation and low codewords redundancy. Furthermore, it is natural to think the better codewords distribution may benefit the generalization and scalability of a retrieval system, i.e., how the system performs under unseen identities in the query stage. It is noteworthy that prior deep hashing works on face image retrieval (Lin et al, 2017; Tang et al, 2018; Xiong et al, 2020; Zhang et al, 2021) only limit their evaluation protocol to seen identities so that the queries used for evaluation share the same classes as the training set. In Sablayrolles et al (2017), researchers have reported that hashing models performing well under this setting may work badly for unseen classes retrieval.

This paper proposes a method called Orthonormal Product Quantization Network (OPQN) to explicitly design codewords and employ them to learn alternative parameters for quantization. Our method predetermines sets of orthonormal vectors as codewords instead of learning them for use. Since the procedure is the opposite of the conventional l2q methods, OPQN belongs to *quantization to learning*.

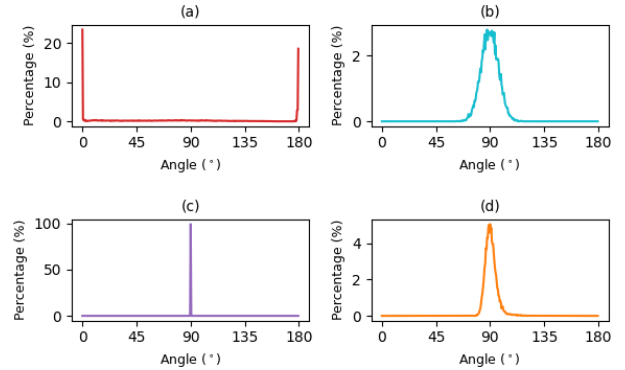


Fig. 1 Distribution of angles between pairs of codewords in different deep quantization models: (a) DPQ (Klein and Wolf, 2019), (b) GPQ (Jang and Cho, 2020), (c) the proposed OPQN method, and (d) the variant of OPQN without predefined codewords. Each angular distribution is a normalized histogram, generated by quantization from 0° to 180° , step by 0.5° .

As shown in Figure 1(c), while other methods exhibit angular distributions of codewords in variations, OPQN produces 90° in 100% of cases. With ℓ_2 normalization on each sub-vector of feature representations, the network learns more separable quantized features composed of predefined codewords in the hyper-sphere space. The main contributions of this paper are summarized in three-fold as followings:

- 1) To the best of our knowledge, we make the first attempt to deploy a deep quantization model producing compact binary codes for large-scale face image retrieval. Our method uses predefined orthonormal vectors as codewords to increase quantization informativeness and reduce codeword redundancy. Besides, it has lower storage costs and more efficient asymmetric comparisons in the retrieval phase.

- 2) We design a tailored loss function, which maximizes discriminability of identities in each subspace. It works simultaneously on the original and the quantized features to give a better quality of quantization. We also impose an entropy-based regularization term to boost the retrieval performance under tiny bits.
- 3) Extensive experiments show that the proposed orthonormal codewords induce consistent and noticeable improvements to model performance and generalization ability. The OPQN method outperforms all compared state-of-the-arts and generalizes the best to retrieve unseen identities. From the further experiments on two general image datasets, the superior performance of OPQN verifies the wide effectiveness of the proposed codewords scheme and the learning metric, providing a general framework for deep quantization-based image retrieval.

Following in this paper, Sect. 2, recalls prior works related to our approach. The proposed OPQN method, including the generation of codewords and design of the loss function are described in Sect. 3. In Sect. 4, OPQN is evaluated on four benchmark datasets: FaceScrub (Ng and Winkler, 2014), CFW-60K (Li et al, 2015), VGGFace2 (Cao et al, 2018), and YouTube Faces (Wolf et al, 2011) under both seen and unseen identities retrieval settings. In Sect. 5, an ablation study with elaboration is reported and the performance of the

model with respect to codebook configurations and parameter sensitivity is discussed. Then, the experiment results on two CIFAR (Krizhevsky et al, 2009) datasets which contain natural images are presented. The paper’s conclusions and outlook for future research are presented in Sect. 6.

2 Related Work

In this section, some representative works on supervised deep hashing are reviewed firstly. Then, traditional quantization and state-of-the-art deep quantization methods for image retrieval are introduced.

2.1 Supervised Deep Hashing for Image Retrieval

Based on the approach of labels utilization, existing supervised deep hashing methods can be roughly classified into three types: pairwise label-based (Li et al, 2016, 2020; Shi et al, 2020), triplet label-based (Wang et al, 2016a; Yao et al, 2016), and class-wise label-based (Zhe et al, 2020; Yuan et al, 2020; Zhang and Yan, 2021). It is known that pairwise label-based methods cannot capture the complete similarity information underlying the whole dataset, and the triplet label-based methods suffer from high computational cost. To address these, Shi et al (2020) proposed an anchor-based self-ensembling method called semi-supervised deep pairwise hashing (SSDPH) that

leverages unlabeled data to preserve similarity relationships. Some works (Zhe et al, 2020; Wang et al, 2020; Yuan et al, 2020) using class-wise label-based similarity were recently proposed, which can generate more discriminative and compact hashing codes.

Previous deep hashing works on face image retrieval mainly focused on the design of the network architecture and widely adopted softmax classification loss for supervision. Specifically, a fully connected (FC) layer transformed bottleneck features to hashing outputs in Euclidean space, which were usually supervised by a softmax classifier. Generally, a quantization loss was also imposed to relax discrete binary constraints to be continuous and to reduce the quantization error. In Discriminative Deep Hashing (DDH) (Lin et al, 2017), deep CNNs were trained with a divide-and-encode module to obtain compact binary codes for face image retrieval. Following DDH, Discriminative Deep Quantization Hashing (DDQH) (Tang et al, 2018) found that retrieval performance can be further enhanced by inserting a batch normalization layer between the FC layer and the Tanh activation function. More recently, several researchers utilized label information with other supervisions. In Deep Discrete Attention Guided Hashing (DAGH) (Xiong et al, 2020), a discrete identity loss effectively compacted intra-identity variations. Inspired from the class-wise

label-based similarity (Zhe et al, 2020), Zhang et al (2021) proposed Deep Center-based Dual-constrained Hashing (DCDH). It used a center-based framework to jointly learn hashing functions and class centers end-to-end, achieving state-of-the-art results on face image retrieval. However, the method could only learn the dataset’s label information and not necessarily capture the underlying semantic similarity of the dataset. This limitation is reflected in the model’s poor generalization performance for unseen identities retrieval in Sect. 4.5.

2.2 Traditional Quantization Techniques

The most classical quantization technique is Vector Quantization (VQ), which quantizes the feature space by maintaining one codebook. Suppose that the codebook consists of K codewords, VQ divides the feature space into K clusters using unsupervised clustering methods, so each feature vector can be encoded by $\log_2 K$ bits. The LUT, which stores the pre-computed distance matrix between every two clusters, has $\mathcal{O}(K^2)$ entries. An increase in VQ’s bit length will lead to exponential growth in the number of clusters, K , and the number of entries in LUT grows quadratically with K , making the method impractical for large values of K and restricting its utility.

PQ (Jegou et al, 2010) overcomes this limitation. It decomposes a feature vector $x_i \in \mathbb{R}^{Md}$ into M disjoint sub-vectors with dimension d , i.e. $x_i = [x_{i1}, x_{i2}, \dots, x_{iM}]$. The sub-vector x_{im} is related to the m -th subspace, which is quantized by the codebook $C_m = [C_{m1}, C_{m2}, \dots, C_{mK}] \in \mathbb{R}^{d \times K}$, composed of K codewords. By representing a feature vector with M codebooks, PQ can achieve K^M combinations of codeword. Therefore, it outperforms VQ with more expressive power for quantization. Optimized PQ methods, such as AQ (Babenko and Lempitsky, 2014) and CQ (Zhang et al, 2014) have been developed to achieve more accurate decomposition of the feature space and learning of codewords. To exploit the provided label information in a supervised manner, Wang et al (2016b) proposed supervised quantization (SQ). However, SQ still conducted feature extraction and quantization steps independently as a traditional quantization approach, which inevitably limited its effectiveness.

2.3 Deep Quantization for Image

Retrieval

Recently, deep quantization methods have emerged as an effective solution for image retrieval tasks, integrating quantization into deep CNNs for simultaneous feature learning and codeword learning. Deep Quantization Network (DQN) (Cao et al, 2016) was the first attempt

in this kind, which introduced a combined similarity-preserving and product quantization loss. Deep Triplet Quantization (DTQ) (Liu et al, 2018) used CQ (Zhang et al, 2014) for quantization and triplet sampling to learn features. Deep Product Quantization (DPQ) (Klein and Wolf, 2019) learned both soft and hard quantizations for a more accurate asymmetric search. It applied a straight-through (ST) estimator to enable back-propagation (BP) on the $\text{argmax}(\cdot)$ function. More recently, Yu et al (2018) proposed product quantization network (PQN), which used a soft PQ layer to directly determine codeword assignments from the cosine similarity between features and codewords. Specifically, both x_{im} and C_{mk} are ℓ_2 normalized to unit length so that their similarity can be taken directly from their inner product. The soft quantization s_{im} of x_{im} in PQN is:

$$s_{im} = \sum_{k=1}^K \frac{e^{\alpha \langle x_{im}, C_{mk} \rangle}}{\sum_{j=1}^K e^{\alpha \langle x_{im}, C_{mj} \rangle}} C_{mk} = \sum_{k=1}^K u_{mk} * C_{mk} \quad (1)$$

where α is a scaling factor. When $\alpha \rightarrow +\infty$, $u_{mk} \rightarrow \mathbb{1}(k = k_*)$, which is a one-hot encoding vector with one in the k_* -th entry and zeros elsewhere. Here, $k_* = \text{argmax}_k x_{im}^T C_{mk}$, represents the index of the most similar codewords for hard quantization. PQN avoids an infeasible derivative caused by $\text{argmax}(\cdot)$, and allows the network

to be optimized by a standard gradient descent algorithm. In [Yu et al \(2020\)](#), researchers further developed RPQN and TPQN, which achieved a higher accuracy for image retrieval and accelerated video retrieval, respectively.

One major problem when employing existing deep quantization methods to face image retrieval tasks is that the applied learning metrics are not sufficiently competent. For example, PQN ([Yu et al, 2018](#)) used an asymmetric triplet loss as the similarity metric and required a complex hard sample mining strategy during training. Moreover, the computational cost is prohibitive when using a large number of triplet samples. Therefore, it cannot learn the full dataset structure of the fine-grained face images. DPQ ([Klein and Wolf, 2019](#)) applied a joint central loss based on classical softmax loss. However, prior works on deep face recognition ([Liu et al, 2017](#); [Wang et al, 2018](#); [Deng et al, 2019](#)) have shown that angular margin-based methods give superior discriminative power for classification. Another problem is what kind of codewords is preferred in deep quantization models for better performance. As shown in [Figure 1](#), previous **l2q** works have significant variations in the distribution of angles between codewords and may be inferior in the quantization informativeness and codewords diversity.

3 Orthonormal Product Quantization

We propose OPQN, a deep quantization-based method specialized for the face image retrieval task. The overview of the training procedure for OPQN is illustrated in [Figure 2](#). We study the functionality of the distribution of codewords in the quantization process, then propose to use sets of predefined orthonormal codewords for quantization. The sub-vectors of deep features are transformed into assignment probabilities via feature-probability decorrelation. Then, they are combined with the predefined codewords to construct the soft quantizations. To provide sufficient discriminative power for PQ-based similarity search, a subspace-wise joint classification loss for the original sub-vectors and their soft quantizations is proposed. Besides, we impose an entropy-based regularization that allows for more precise quantization.

The notations used in this paper are introduced as follows. We denote a dataset with N face images as $\{I_i\}_{i=1}^N$, and the corresponding label vector as $y \in \mathbb{R}^N$. For an input image I_i , $x_i \in \mathbb{R}^D$ is the bottleneck features as shown in [Figure 2](#) produced by the backbone network $f(\Theta)$, where Θ are the backbone network parameters. x_i is divided into M disjoint sub-vectors with dimension $d = D/M$, i.e., $x_i = [x_{i1}, x_{i2}, \dots, x_{iM}]$ where $x_{im} \in \mathbb{R}^d$. Assume the

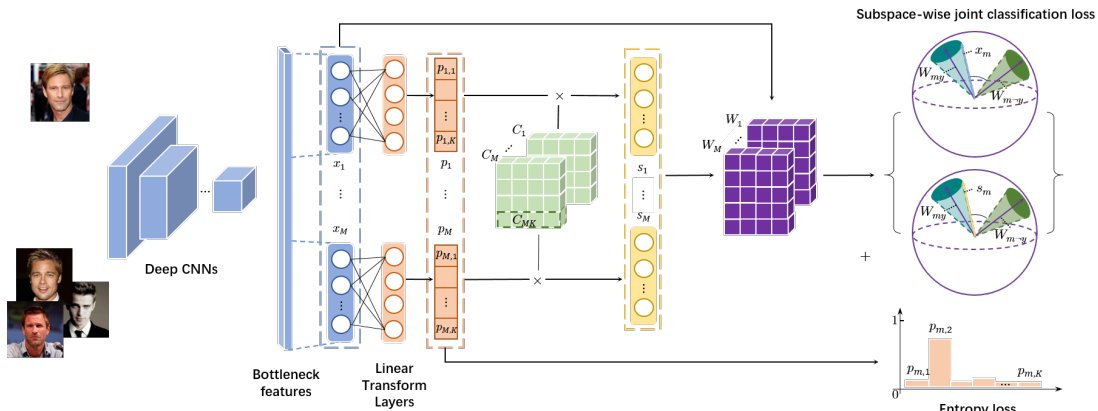


Fig. 2 The overall training procedure of the OPQN method: x_m represents the sub-vector from the bottleneck features. x_m is projected by a linear transform layer followed by a softmax operation to produce the probability vector p_m . The soft quantization s_m is constructed as a convex combination between p_m and the orthonormal codewords C_m . W_m represents the weight matrix of the subspace-wise classification loss. The discriminability of x_m and s_m in each subspace is maximized by the classification loss. An entropy loss is added to p_m as a regularization term that allows for more precise quantization.

codebooks $C = [C_1, C_2, \dots, C_M] \in \mathbb{R}^{M \times d \times K}$ and each codebook consists of K codewords, i.e., $C_m = [C_{m1}, C_{m2}, \dots, C_{mK}] \in \mathbb{R}^{d \times K}$. The soft and hard quantizations of x_{im} are s_{im} and h_{im} , respectively. Concretely, $h_{im} = C_{mk_*}$, is the approximation of x_{im} by the codeword with index k_* in m -th codebook. Thus, the soft and hard quantizations of I_i can be represented as $s_i = \{s_{im}\}_{m=1}^M$ and $h_i = \{h_{im}\}_{m=1}^M$, respectively.

3.1 Soft Quantization via Feature-Probability Decorrelation

The soft quantization shown in Eq. (1) implicitly encodes the similarity between sub-vectors and codewords. Consequently, how each codeword constitutes s_{im} , and how far the distance between s_{im} and C_{mk_*} is, are both difficult to observe. As the scaling factor cannot be set to positive

infinity, there is always a gap between s_{im} and h_{im} . Alternatively, OPQN learns the codewords assignment explicitly via an intermediate fully connected layer. Note that since the codewords are now predefined, it offsets the number of parameters in the intermediate layer. Thus, the total number of learnable parameters does not grow. Inspired by DPQ (Klein and Wolf, 2019), a linear transformation layer is built on top of each sub-vector x_{im} individually. The parameter matrices in all linear transform layers are denoted as $F = [F_1, F_2, \dots, F_M] \in \mathbb{R}^{M \times d \times K}$. For simplicity, we omit the biases in each layer. By appending a softmax function to layer outputs, we can formulate the probability of assigning the codeword C_{mk} to the subvector x_{im} as:

$$p_{im,k} = \frac{e^{x_{im}^T F_{mk}}}{\sum_{j=1}^K e^{x_{im}^T F_{mj}}} \quad (2)$$

where F_{mj} is the j -th column of the parameter matrix F_m . The K probabilities are concatenated to the vector: $p_{im} = [p_{im,1}, p_{im,2}, \dots, p_{im,K}] \in \mathbb{R}^K$. The soft quantization s_{im} of x_{im} in the proposed method is represented as:

$$s_{im} = \sum_{k=1}^K p_{im,k} * C_{mk} \quad (3)$$

Eq. (3) means each soft quantization s_{im} is the convex combination of $\{C_{mk}\}$ with softmax coefficients p_{im} . Based on this, one can naturally derive the hard quantization as $h_{im} = C_{mk_*}$. Here, k_* is the index of the codeword with the largest value in p_m^i , formulated as:

$$k_* = \underset{k}{\operatorname{argmax}} p_{im,k} \quad \text{s.t.} \quad k = 1, 2, \dots, K \quad (4)$$

Note that the proposed method does not compute the hard quantization in the training process, which avoids the problem of calculating the derivative of $\operatorname{argmax}(\cdot)$. Eq. (4) serves to encode database items during the testing query phase, which will be detailed in Sect. 3.6.

3.2 Orthonormal Codewords

Generation

The above soft quantization method connects the sub-vectors and codewords by learning a linear transform matrix to explicitly represent the quantization composition. Thus, it is feasible to use predefined codewords for quantization. Assume

there is a codebook C_m , with each column being a codeword. For any pair of codewords C_{mi} and C_{mj} : $0 \leq \angle(C_{mi}, C_{mj}) \leq \pi$. The basic idea of codeword design is to improve the informativeness of quantization as well as reduce the redundancy in the codewords. We require each pair of codewords to have a sufficiently large angle between them and the variance of angles, $\angle(C_{mi}, C_{mj})$ to be as small as possible. To eliminate side effects caused by the magnitudes, C_{mi} and C_{mj} should be normalized to unit length. In terms of these requirements, we apply the orthonormal vectors as codewords, which possess the following desirable characteristics:

- $\|C_{mk}\| = 1$
- $C_m^T C_m = I_K$

The orthonormal vectors are naturally of unit norm and every two different orthonormal vectors keep a $\pi/2$ angular separation from each other.

There are some other choices to generate a set of orthonormal vectors. For example, one can perform Singular Value Decomposition (SVD) on a random matrix and return the columns of the left-singular vectors as codewords. However, a better solution is to use deterministic orthonormal vectors that excludes the randomness biases caused by codewords themselves. Thereby, we utilize the cosine basis of Discrete Cosine Transform

(DCT) (Ahmed et al, 1974), in the DCT-II algorithm. Since DCT-II is defined by a set of orthogonal/orthonormal cosine basis functions, one can always obtain the exactly same orthonormal vectors if only the dimension is specified. Suppose the dimension of sub-vectors, as well as codewords, are d , the basis matrix $A \in \mathbb{R}^{d \times d}$ in the DCT-II transform can be calculated as:

$$A_{ij} = \cos\left[\frac{j\pi}{d}\left(i + \frac{1}{2}\right)\right] \quad s.t. \ i, j = 0, 1, 2, \dots, d-1 \quad (5)$$

The procedure to generate orthonormal codewords using the cosine basis is summarized in Algorithm 1. By several processing steps (steps 2 and 3) on A , we could obtain an orthogonal matrix A^\dagger , whose first K column vectors are the desired codewords in one codebook. The orthonormal vectors multiplied by an orthogonal matrix are still orthonormal vectors. Thus, we iteratively multiply the previous codebook by A^\dagger to get the new codebook, which guarantees the diversity between different sets of codebooks while still retaining the orthogonality of each codebook. One thing noted that OPQN requires that the number of codewords is no more than the dimension of the sub-vectors. For a network with a bottleneck of 2048-dimensional features, it can generate binary codes up to 64-bit ($8 \log_2 256$) in length, which is sufficient to cover most cases.

Algorithm 1 Generation of deterministic orthonormal codewords

Input: Dimension of feature representations D , number of codebooks M , number of codewords per codebook K , dimension of sub-features d , where $d = D/M$ and $K \leq d$

Output: Codebooks $C \in \mathbb{R}^{M \times d \times K}$

- 1: Compute the cosine basis matrix A according to Eq. (5)
 - 2: $A[:, 0] \leftarrow A[:, 0]/\sqrt{2}$
 - 3: $A^\dagger \leftarrow \sqrt{2}A/\sqrt{d}$
 - 4: $C_1 = A^\dagger[:, :K]$
 - 5: **for** $m = 2 : M + 1$ **do**
 - 6: $C_m = A^\dagger * C_{m-1}$
 - 7: **end for**
-

3.3 Subspace-Wise Joint

Classification Loss

By substituting the codewords in Eq. (3) with the predefined orthonormal codewords generated by Algorithm 1, we can obtain the soft quantization of feature vectors in each subspace. These quantized features will be fed into the carefully designed objective function supervised with label information for discriminative face image retrieval. Nevertheless, it is natural that the bottleneck features directly limit the quantization performance. The well-learned original features should benefit the embedding of identity-specific clues in quantized features. Therefore, we propose to preserve the discriminability in both the original and soft quantized features.

From another view, since the original features and their quantized versions fall into several disjoint subspaces in PQ-based methods, the associated full identity information also breaks into

different partitions. For better classification, we expect intra-identity features and their soft quantizations to be separable from those belonging to other identities in each subspace. Thus, a set of subspace-wise classifiers can be learnt individually for each segment of x_{im} and s_{im} .

We denote a fully connected layer containing a set of weight matrices as $W = [W_1, W_2, \dots, W_M] \in \mathbb{R}^{M \times d \times C}$, where C is the number of identity classes in the datasets. W_{mc} represents the c -th column vector of W_m in the m -th subspace. We normalize W_{mc} : $W_{mc} \leftarrow W_{mc} / \|W_{mc}\|_2$ that is commonly used in deep face recognition. Correspondingly, x_{im} is also ℓ_2 normalized: $x_{im} \leftarrow x_{im} / \|x_{im}\|_2$. Thus, the cosine similarity between x_{im} and W_{mc} is directly implied from their inner product. Specifically, $\cos \theta_{y_i, x_{im}} = x_{im}^T W_{my_i}$, where $\theta_{y_i, x_{im}}$ represents the angle between x_{im} with label y_i and its corresponding weight vector W_{my_i} . Inspired by the popular and effective line of angular margin-based deep face recognition (Wang et al, 2018; Deng et al, 2019), we add a cosine margin u between $\cos \theta_{y_i, x_{im}}$ and $\cos \theta_{y_{-i}, x_{im}}$. The introduced margin helps to enhance the intra-identity compactness and inter-class discriminability of the original features in each subspace. By formulating the angular margin into the softmax classification loss and summing up the loss terms coming from all the M segments, we obtain the loss function

concerning x and W as:

$$L_x = \sum_{i=1}^N \sum_{m=1}^M -\log \frac{e^{r(\cos \theta_{y_i, x_{im}} - u)}}{e^{r(\cos \theta_{y_i, x_{im}} - u)} + \sum_{j \neq y_i} e^{r \cos \theta_{j, x_{im}}} \quad (6)$$

where r is a scaling factor for the normalized sub-features. We also ℓ_2 normalize s_{im} to remove the variation in the radius. Then, the cosine distance between s_{im} and W_m is indicated by their multiplication, and the angle between s_{im} and W_{my_i} is denoted as $\theta_{y_i, s_{im}}$. Similarly, the angular margin-based loss function w.r.t. s and W is formulated as:

$$L_s = \sum_{i=1}^N \sum_{m=1}^M -\log \frac{e^{r(\cos \theta_{y_i, s_{im}} - u)}}{e^{r(\cos \theta_{y_i, s_{im}} - u)} + \sum_{j \neq y_i} e^{r \cos \theta_{j, s_{im}}} \quad (7)$$

The values of margin u and scaling factor r in Eq. (7) are the same as in Eq. (6) to encourage consistency between x_{im} and s_{im} . Combining Eq. (6) and Eq. (7), the joint similarity-preserving loss is represented as:

$$\min_{\Theta, F, W} L_{clf} = \frac{1}{2MN} (L_x + L_s) \quad (8)$$

Eq. (8) targets subspace-wise intra-identity variance minimization and inter-identity variance maximization for both the original and quantized features.

3.4 Entropy Minimization for

One-Hot Codewords Assignment

The joint classification loss with regularization utilized soft quantization s_{im} without considering hard quantization h_{im} in training. However, we would like to reduce the discrepancy between s_{im} and its corresponding original version h_{im} . The probability vector p_{im} , which takes the role of codewords assignment, should be close to one-hot encoding. Therefore, we propose an entropy-based regularization term to force the learned sub-feature to move towards a single codeword while pushing it apart from other codewords. The entropy-based loss is formulated as:

$$L_{ent} = -\frac{1}{MN} \sum_{i=1}^N \sum_{m=1}^M \sum_{k=1}^K p_{im,k} \log p_{im,k} \quad (9)$$

$p_{im,k} \log p_{im,k}$ has the minimum value 0 if and only if $p_{im,k} = 0$ or $p_{im,k} = 1$. Under the constraint of $\sum_k p_{im,k} = 1$, the proposed entropy loss tends to shape the distribution of p_{im} into a pattern with a single peak at one index with small values elsewhere. By adding the loss terms from all the M probability vectors, it accomplishes discrepancy reduction between s_i and h_i for more precise quantization. By integrating L_{clf} and L_{ent} , we get the finalized loss function of OPQN:

$$L = L_{clf} + \lambda L_{ent} \quad (10)$$

where λ is a balance weight of the entropy loss.

3.5 Learning and Optimization

The proposed OPQN contains three sets of learnable parameters: backbone network parameters Θ , linear transform layer parameters F and the classification weight W . We adopt the mini-batch strategy and stochastic gradient descent (SGD) in training and all parameters can be learned by back-propagation (BP). Denote x_{im}^T multiplied by F_m shown in Eq. (2) as $g_m = [g_{m1}, g_{m2}, \dots, g_{mK}]$. The gradients of p_{im} w.r.t g_m can be computed as:

$$\frac{\partial p_{im,k}}{\partial g_{mk}} = p_{im,k}(1-p_{im,k}); \quad \frac{\partial p_{im,k}}{\partial g_{mj}(j \neq k)} = -p_{im,k}p_{im,j} \quad (11)$$

Thus, we can derive the gradient of the soft quantization s_{im} w.r.t. g_{mk} by BP:

$$\frac{\partial s_{im}}{\partial g_{mk}} = \left[\frac{\partial s_{im}}{\partial p_{im}} \right]^T \frac{\partial p_{im}}{\partial g_{mk}} = p_{im,k}(C_{mk} - s_{im}) \quad (12)$$

Similarly, since $\partial L_{ent} / \partial p_{im} = -(1 + \log p_{im})$, we obtain the derivatives of L_{ent} w.r.t. g_{mk} using Eq. (11) as:

$$\frac{\partial L_{ent}}{\partial g_{mk}} = p_{im,k} \left(\sum_{j=1}^K p_{im,j} \log p_{im,j} - \log p_{im,k} \right) \quad (13)$$

Algorithm 2 OPQN Training Procedure

Input: Training set $\{I_i\}_{i=1}^N$ with labels y , the network $f(\cdot)$, the dimension of codebooks: $M \times d \times K$;
Initialization: Backbone network parameters Θ , linear transform layer F , classification weight matrix W ;

- 1: Generate orthonormal codewords by Algorithm 1;
- 2: **repeat**
- 3: Randomly sample a mini-batch data from training set;
- 4: Feed forward the mini-batch images through the model and compute $x_i = f(\Theta; I_i)$ for each image;
- 5: Calculate the objective function L according to Eq. (10);
- 6: Compute the derivatives of L w.r.t. W , F and x_{im} according to Eq. (15), Eq. (14) and Eq. (16), respectively;
- 7: Back propagate the gradients to the backbone network, then update the parameters W , F and Θ ;
- 8: **until** Convergence

Combining Eq. (12) and Eq. (13) and applying BP, the derivative of L regarding F_{mk} is:

$$\frac{\partial L}{\partial F_{mk}} = \left[\frac{1}{2} \left(\frac{\partial L_s}{\partial s_{im}} \right)^T \frac{\partial s_{im}}{\partial g_{mk}} + \lambda \frac{\partial L_{ent}}{\partial g_{mk}} \right] x_{im} \quad (14)$$

Likewise, the derivative of L regarding W is calculated by:

$$\frac{\partial L}{\partial W_{mk}} = \frac{1}{2} \left(\frac{\partial L_x}{\partial W_{mk}} + \frac{\partial L_s}{\partial W_{mk}} \right) \quad (15)$$

The derivative of L w.r.t. x_{im} is:

$$\frac{\partial L}{\partial x_{im}} = \frac{1}{2} \frac{\partial L_x}{\partial x_{im}} + \frac{1}{2} \left(\frac{\partial L_s}{\partial g_{mk}} + \lambda \frac{\partial L_{ent}}{\partial g_{mk}} \right) F_{mk} \quad (16)$$

The complete training procedure of OPQN is summarized in Algorithm 2.

3.6 Asymmetric Distance

Comparison for Retrieval

Following previous works (Yu et al, 2018; Klein and Wolf, 2019; Yu et al, 2020; Jang and Cho, 2020), we apply asymmetric quantization distance (AQD) (Jegou et al, 2010) as the similarity metric in the search phase. AQD enables using soft quantizations to represent a query but hard quantizations to encode database images. It has the advantages of both memory footprint reduction and retrieval speed acceleration. To this end, the query and database items in the search phase are handled with different processing procedures.

Given a query image q , we propagate it through the model until the linear transform layers. These outputs are passed to the softmax function, as in Eq. (2), to obtain the probability vector p_{qm} of each subvector x_{qm} . Then, combined with C_m to obtain the soft quantization s_{qm} , as in Eq. (3). For each database image I_i , we pre-compute $\{p_{im}\}$ following the same procedure as the query image. I_i is associated with its hard quantization $\{h_{im}\}$ via the indices of the largest values in $\{p_{im}\}$. Suppose that we have a matrix $B \in \mathbb{R}^{N \times M}$, then each element b_{im} of B stores the index k_* of codewords in Eq. (4). Therefore, the Euclidean distance between q and I_i , is computed

as:

$$\begin{aligned} AQD(q, I_i) &= \sum_{m=1}^M \|s_{qm} - h_{im}\|_2^2 \\ &= \sum_{m=1}^M \|C_m p_{qm} - C_{mb_{im}}\|_2^2 \end{aligned} \quad (17)$$

Note the orthogonality of C_m . By expanding the right-hand side of Eq. (17) and eliminating the constant and the term irrelevant to $C_{mb_{im}}$, we can derive the following equation:

$$\begin{aligned} \operatorname{argmin}_i AQD(q, I_i) &= \operatorname{argmin}_i \sum_{m=1}^M -2p_{qm}^T C_m^T C_{mb_{im}} \\ &= \operatorname{argmax}_i \sum_{m=1}^M p_{qm, b_{im}} \end{aligned} \quad (18)$$

From Eq. (18), $\operatorname{argmin}_i AQD(q, I_i)$ depends on $\{p_{qm}\}_{m=1}^M$ and $\{b_{im}\}_{m=1}^M$. It indicates the quantization similarity comparison between the query and any database item can be realized efficiently by indexing p_{qm} with LUTs. Specifically, we build M LUTs, denoted as $\{LUT_m\}$, w.r.t. M probability vectors $\{p_q\}$, where $LUT_m[i] = b_{im}$. Since the matrix B can be pre-computed, it only takes several addition calculations in the searching process. Compared with other PQ methods, OPQN has two advantages. Firstly, unlike DQN (Cao et al, 2016) and DPQ (Klein and Wolf, 2019), OPQN does not require explicit online reconstruction of the soft quantization or calculation of the

Algorithm 3 OPQN Top- k Retrieval Procedure

Input: Database images $DB = \{db_i\}_{i=1}^{|DB|}$, query set images $Q = \{q_i\}_{i=1}^{|Q|}$, the trained model;

Output: Top k instances in DB for each q_i ;

- 1: Forward pass DB through the model in advance, and pre-compute the indices matrix B according to Eq. (2) and Eq. (4);
 - 2: LUTs construction for DB based on matrix B ;
 - 3: **for** i in $1, 2, \dots, |Q|$: **do**
 - 4: Forward pass q_i through the model and compute $p_{q_i, m}$ by Eq. (2);
 - 5: Compute similarity between q_i and each database image by Eq. (18) using LUTs, and sort the results in descending order;
 - 6: Return top k instances in DB
 - 7: **end for**
-

Euclidean distance between the soft quantization and each codeword. Therefore, it is more scalable and time-efficient to handle a query which arrives on-the-fly. Secondly, the codebooks in our method are data-independent and predefined. This allows models to use the same codebook for different datasets, helping to lower the system's storage cost. The retrieval procedure of OPQN is summarized in Algorithm 3.

4 Experiments and Results

4.1 Datasets and Evaluation Metrics

To demonstrate the performance of the proposed OPQN, we conduct experiments on four commonly-used publicly available datasets: FaceScrub (Ng and Winkler, 2014), CFW-60K (Li et al, 2015), VGGFace2 (Cao et al, 2018), and YouTube Faces (Wolf et al, 2011). For simplicity, we refer the evaluation of seen identities to

standard retrieval. The details of each dataset and their corresponding protocols are:

4.1.1 FaceScrub

FaceScrub (Ng and Winkler, 2014) contains 106,863 face images of 530 celebrities with about 200 images per identity. We use the same training-testing split as in Lin et al (2017); Tang et al (2018): five images per identity are selected for testing, and the remaining images are used for training. All the face images have been cropped and resized to 32×32 .

4.1.2 CFW-60K

CFW-60K (Li et al, 2015) is a dataset containing 60,000 images of 500 identities. As in Zhang et al (2021), we use the official test split in CFW-60K, which has 10 images per identity and a total of 5000 images for testing. Among the other images, a total number of 55,000 images with category labels were used for training. All the face images have the same size of 32×32 .

4.1.3 VGGFace2

The official VGGFace2 (Cao et al, 2018) dataset contains 3.31 million images of 9,131 identities, split into 8,631 identities for training and 500 identities for testing. The identities in the training testing split are disjoint. We choose 2,787 identities, with approximately 300 images each, from the official training set. 50 images per identity

were taken from those 2,787 classes for testing, with the rest used for training. Under the standard retrieval protocol, the training set is employed as the database while the testing set is used as queries. In the unseen identities retrieval protocol, we take all the identities in the official testing set. 50 images per identity are used as queries, with the remainder used as a database. All the images in VGGFace2 are cropped and aligned following the instructions of MTCNN (Zhang et al, 2016). Each image is resized to 112×112 .

4.1.4 YouTube Faces

YouTube Faces (Wolf et al, 2011) contains thousands of videos of 1,595 celebrities. The duration of each video ranges from 48 frames to 6,070 frames. Following the configuration in Lin et al (2017), we select 40 images per identity for training and 5 images for testing. The employed dataset has 63,800 training images and 7,975 testing images. Each image is resized to 32×32 . Since YouTube Faces is relatively simple compared to others and the standard retrieval performance is nearly saturated, as shown in Zhang et al (2021), we only evaluate unseen identities retrieval on this dataset.

For seen identities retrieval, the training-testing split is used as database images and queries, respectively, for each dataset. Three kinds of evaluation metrics are applied to evaluate the quality of the retrieval: mean average precision

(MAP), precision-recall (PR) curve, and precision w.r.t. top T returned images ($P@T$).

4.2 Experiment Settings

We compare OPQN with a series of binary hashing-based and PQ-based methods. The deep hashing methods include DDQH (Tang et al, 2018), DCWH (Zhe et al, 2020), CSQ (Yuan et al, 2020), DCDH (Zhang et al, 2021), and DPAH (Wang et al, 2020). Among them, DDQH and DCDH are originally developed for face image retrieval, while others aim at general image retrieval tasks. Since DDQH and DCDH methods in their papers apply different backbone networks from OPQN, we denote the original results as DDQH and DCDH, while our unified implementations as DDQH* and DCDH*, respectively. For PQ-based methods, we compare OPQN with DPQ (Klein and Wolf, 2019) and GPQ (Jang and Cho, 2020), which are both initially designed for general image retrieval. We also present the result of the variant of OPQN, OPQN-l2q, which employs the same learning metric as OPQN, but learns codewords instead of predetermining them, as in DPQ and GPQ.

To ensure a fair comparison, we unify the backbone network for all the binary hashing and PQ-based methods. Thus, the difference in the networks between binary hashing and PQ-based methods only exists in the last few layers, which

distinguish the approaches from each other. Without loss of generality, the employed backbone network is based on the ResNet20 (He et al, 2016) architecture, shown in Figure 3. Similar architectures have been used in prior deep face recognition works (Liu et al, 2017; Deng et al, 2019). As illustrated in Figure 3, for quantization-based methods, the outputs of the last convolutional layer are flattened and projected into the FC1 layer to generate the bottleneck features shown in Figure 2. In contrast, for hashing-based methods, the flattened convolutional layer’s outputs are first transformed into 512-dimensions by the FC1 layer, followed by an FC hashing layer to produce hashing outputs with expected code length. We apply dropout (Srivastava et al, 2014) to the flatten layer, and batch normalization (Ioffe and Szegedy, 2015) is used after each fully connected layer in both methods.

4.3 Implementation Details

We evaluate the performance of OPQN under code lengths ranging from 16 to 64 bits. During training, OPQN uses a mini-batch SGD algorithm for optimization with momentum of 0.9 and weight decay of $5e-4$. For small datasets, i.e., FaceScrub (Ng and Winkler, 2014) and CFW-60K (Li et al, 2015), the initial learning rate is set to 0.1 and decayed by 0.5 every 35 epochs, while in VGGFace2 (Cao et al, 2018) dataset, the initial learning rate is set to 0.01 and decayed by 0.5 every 20 epochs. The batch size is fixed to 256 for

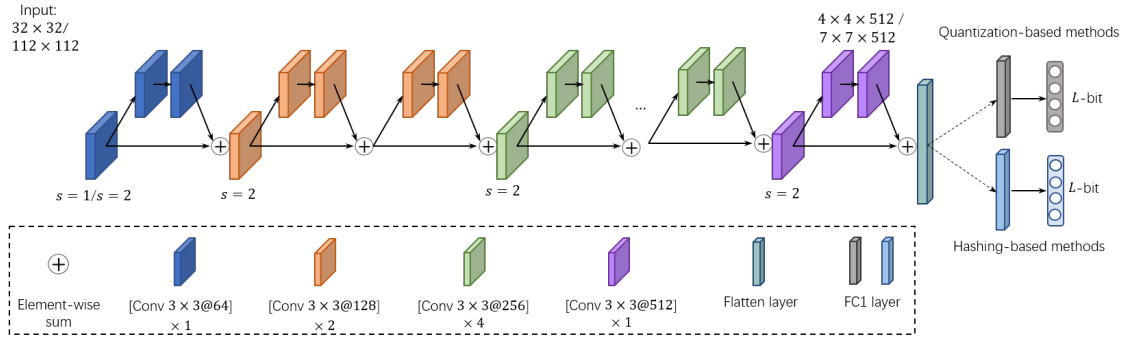


Fig. 3 The applied network with ResNet20 architecture. ‘[Conv3 × 3@ ϕ] × ψ ’ represents a number of stacked ψ residual blocks with a kernel size of 3 × 3 that output ϕ -channel feature maps. The first convolutional layer of the first block applies a unit stride, or a stride of 2, depending on the input size, as separated by ‘/’, respectively, while the first layers in other blocks were all performed with a stride of 2 for down-sampling.

all datasets, and the whole network is trained for 200 epochs. From cross-validation, the parameter settings for OPQN are: the scaling factor $r = 40$, the margin $u = 0.4$, and the balance weight $\lambda = 0.1$. We apply the same data augmentation process to all methods during training: the images are firstly enlarged to about 1.1 times the original input size. Then, they are randomly cropped to the original size with random horizontal flipping. Experiments of the compared methods use the codes available from the original authors if possible. Otherwise, we carefully implement the methods. All experiments are performed on two Nvidia RTX-2080 GPU cards and implemented with PyTorch (Paszke et al, 2019).

4.4 Seen Identities Retrieval

We first conduct experiments on the proposed OPQN with the FaceScrub and CFW-60K datasets, following the standard retrieval protocol in prior works. We evaluate the binary codes

under 16, 24, 36, and 48 bits, with the number of codebooks, M , set empirically to 2, 4, 6, and 8, respectively. Thus, the number of codewords in each codebook, K , are accordingly 256, 64, 64, and 64. Note that the bottleneck features, with dimension D , should fulfill the conditions $D/M \leq K$ and $D \mid M$. For simplicity, we fix D to 512 for all cases except 36 bits where D is set to 516 to be divisible by the number of codebooks, i.e., 6. The other PQ-based methods adopt the same codebook and codeword settings as the proposed OPQN.

The MAP results on FaceScrub and CFW-60K datasets are summarized in Table 1. OPQN outperforms all the other methods over all code lengths. OPQN achieves average performance improvements of 3.83% and 2.26% over the state-of-the-art deep hashing method DCDH* on the FaceScrub and CFW-60K datasets, respectively. The superiority of OPQN is more prominent under short code lengths. For example, under 16-bit codes, it outperforms the second place

Table 1 MAP results on FaceScrub, CFW-60K, and VGGFace2 datasets under the standard retrieval setting

Method	FaceScrub				CFW-60K				VGGFace2			
	16-bit	24-bit	36-bit	48-bit	16-bit	24-bit	36-bit	48-bit	24-bit	36-bit	48-bit	64-bit
DDQH	-	0.4482	0.5071	0.5191	-	-	-	-	-	-	-	-
DDQH*	0.8393	0.8561	0.8714	0.8828	0.7832	0.7880	0.8069	0.8222	0.8119	0.9014	0.9167	0.9289
DCWH	0.8352	0.8445	0.8562	0.8872	0.7014	0.7251	0.7480	0.7839	0.3423	0.5224	0.6458	0.7259
DPAH	0.8398	0.8859	0.9006	0.9041	0.7602	0.8266	0.8399	0.8454	0.8159	0.8715	0.8897	0.9042
CSQ	0.7123	0.8032	0.8206	0.8661	0.6969	0.7219	0.7844	0.8335	0.7072	0.7934	0.8304	0.8371
DCDH	-	0.7779	0.8347	0.8464	-	0.8168	0.8356	0.8548	-	-	-	-
DCDH*	0.8496	0.8718	0.8953	0.9143	0.8055	0.8608	0.8669	0.8716	0.8752	0.9095	0.9181	0.9232
DPQ	0.3870	0.8405	0.9043	0.9071	0.3043	0.5761	0.7037	0.7055	0.7105	0.7703	0.8435	0.8681
GPQ	0.6338	0.8036	0.8593	0.8699	0.6402	0.4931	0.6146	0.7190	0.6790	0.7041	0.7286	-
OPQN (Ours)	0.9032	0.9154	0.9270	0.9385	0.8547	0.8637	0.8826	0.8940	0.8986	0.9508	0.9504	0.9529
OPQN-l2q	0.6273	0.8971	0.9162	0.9254	0.5278	0.8351	0.8725	0.8780	0.7600	0.8575	0.9127	0.9059

DCDH* by a margin of 5.36% and 4.92% on two datasets, respectively. It proves the feasibility of quantization-based face image retrieval.

The other deep quantization models, DPQ and GPQ, do not perform as well as deep hashing-based methods. Particularly, the performances of DPQ and GPQ are poor for 16-bit codes. This may be due to their applied learning metrics being insufficient to extract discriminative features given that the complete visual information attached to the feature vector is divided into several subspaces. In contrast, OPQN maximizes the discriminability of both soft representations and sub-vectors in each subspace and so is competitive in this situation. It is worth noting that the variant, OPQN-l2q, performs worse than OPQN, with relatively minor decreases for 24 to 48 bit codes but is 27.59% and 32.69% lower for the 16 bit codes on FaceScrub and CFW-60K, respectively. The results strongly support the effectiveness of

the proposed orthonormal scheme. As shown in Figure 1, we plot the angular distribution of pairwise codewords of four methods on FaceScrub under 16-bit codes. Figure 1 implies that the orthonormal codewords contribute to better preserving the visual information in the subspace, by which the codewords are evenly distributed with a specific and moderate (90 degrees) separation from each other.

We further conduct experiments on the employed VGGFace2 dataset under four code lengths, 24, 36, 48, and 64 bits. The number of codebooks are set to 3, 4, 6, and 8, respectively. Accordingly, the number of codewords in each codebook is 256 except for the 36 bit case where it is 512. The dimension D of the bottleneck features in OPQN is set to $D = MK$. For a fair comparison, the DPQ (Klein and Wolf, 2019) method is evaluated with the same configuration of D , M , K , while the GPQ (Jang and Cho, 2020) method,

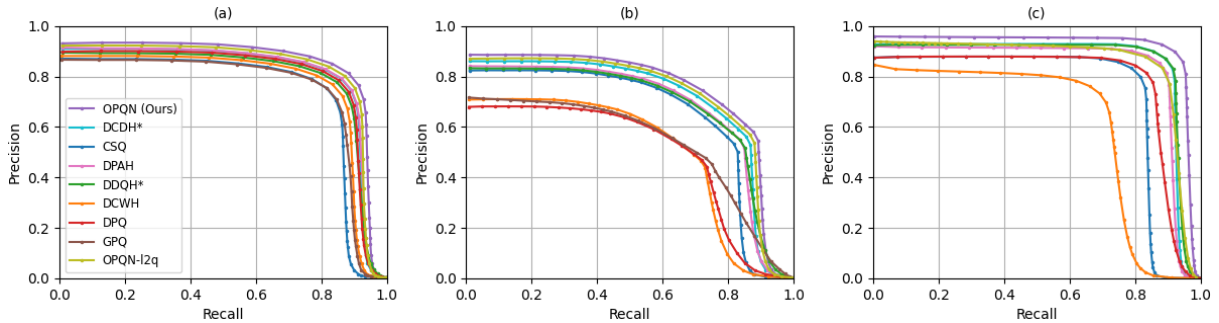


Fig. 4 Performance measured by PR-curves: (a) 48-bit codes on FaceScrub, (b) 48-bit codes on CFW-60K, (c) 64-bit codes on VGGFace2.

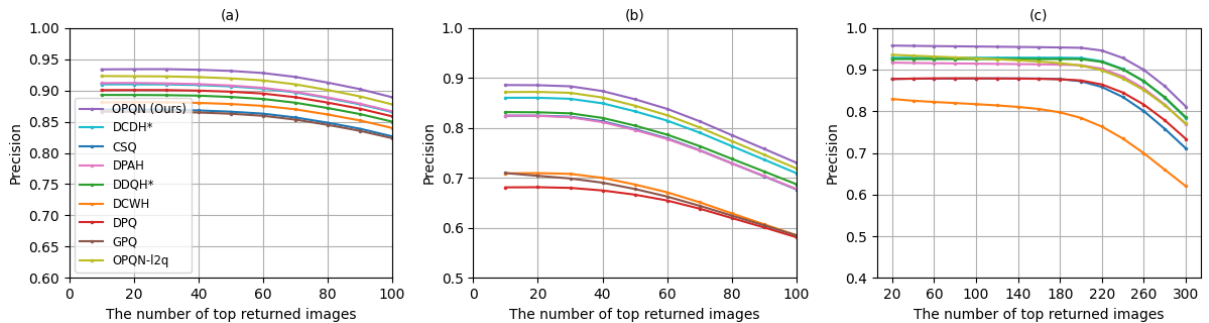


Fig. 5 Performance w.r.t. different P@T on three datasets: (a) 48-bit codes on FaceScrub, (b) 48-bit codes on CFW-60K, (c) 64-bit codes on VGGFace2.

could only perform well with a large value of K in this case. Thus, we fix K as 4096 (2^{12}), and M as 2, 3, and 4 to obtain 24 bit, 36 bit, and 48 bit codes, respectively. We adopt $D = 2048$ for 24 and 48 bit codes, and 2049 for 36 bit codes. The 64 bit result for GPQ is not show as it does not support a reasonably large value of K .

The MAP performance on the VGGFace2 subset is shown in the right part of Table 1. It is clear that OPQN outperforms all the other methods over all code lengths, exceeding the two best competitors, DCDH (Zhang et al, 2021) and DDQH (Tang et al, 2018), by 3.18% and 4.85% on average, respectively. At 36 bits, OPQN's more

than 95% MAP is 4.13% higher than the second place DCDH*. There is a noticeable drop in the performance from OPQN to the variant method OPQN-l2q. OPQN-l2q and DPQ have much poorer performance than their hashing-based counterparts, DCDH* and DDQH*, especially at 24 bits. Once again, the results indicate that l2q-based methods, which ignore the code-words' inherent angular distribution, suffer from poor quantization quality when the original feature space is divided into only a few subspaces. Besides, the general task-oriented loss functions are insufficient to draw powerful feature representations or integrate all the visual information in each subspace for quantization.

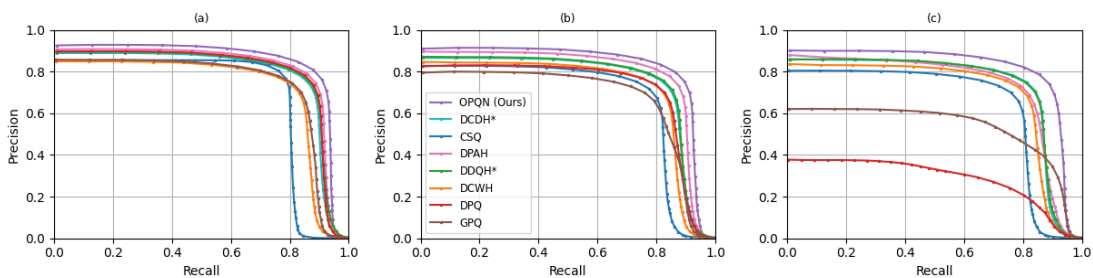


Fig. 6 PR curve performance on the FaceScrub dataset w.r.t different code lengths: (a) 36-bit, (b) 24-bit, (c) 16-bit.

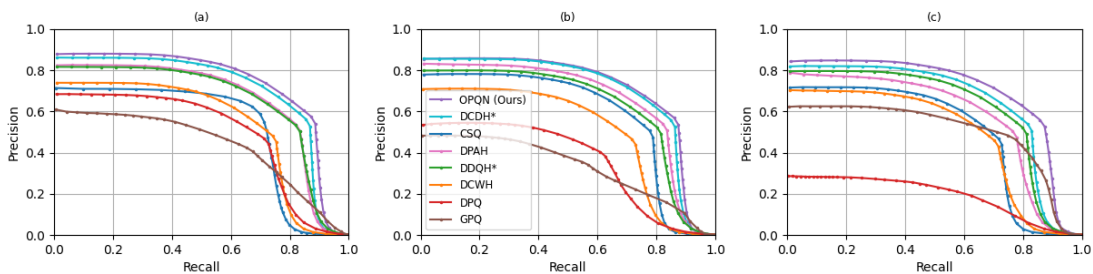


Fig. 7 PR curve performance on the CFW-60K dataset w.r.t different code lengths: (a) 36-bit, (b) 24-bit, (c) 16-bit.

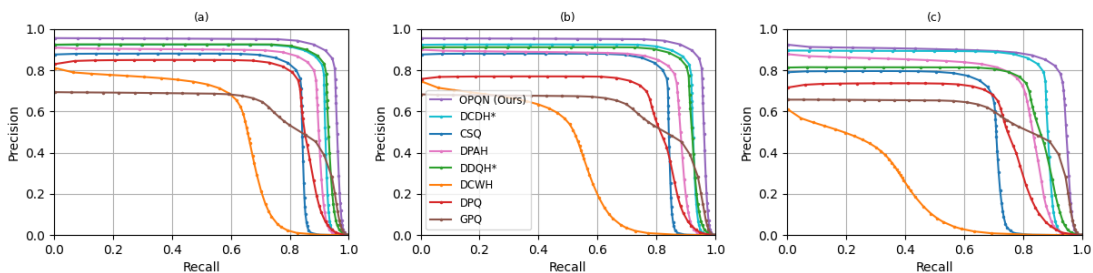


Fig. 8 PR curve performance on the VGGFace2 dataset w.r.t different code lengths: (a) 48-bit, (b) 36-bit, (c) 24-bit.

We then evaluate the performance on the PR-curve as shown in Figure 4. We can see that the PR-curves of OPQN almost always span outermost from the top-left to the bottom-right corner of the whole figures for three datasets. This means that OPQN can maintain a higher precision with the increase in the recall score. Since face image retrieval system users generally only look at top ranking images, it is also necessary to evaluate the retrieval accuracy in terms of a different numbers of top returned images. Therefore, we plot

$P@T$ curves w.r.t. different t on the three datasets in Figure 5. OPQN consistently achieves the best precision compared to other methods, verifying its capability of providing superior retrieval results over a moderate quantity of returns. Specifically, we compute $P@T$ for up to 300 images in VGGFace2, which is the average number of images belonging to one identity in the database. OPQN is the only method that maintains higher than 80% precision in the top 300 positions. Considering the large pose and age variations

in the VGGFace2 dataset, retrieving more than 80% of related images is satisfying. Combining the results with MAP and PR-curves, this shows that OPQN is robust to different evaluation metrics. The comparisons of the PR-curves w.r.t. other code lengths on the FaceScrub, CFW-60K, and VGGFace2 datasets, are shown in Figures 6, 7, and 8, respectively.

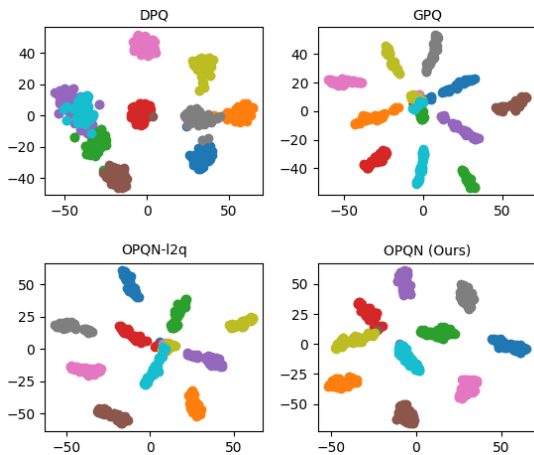


Fig. 9 Visualization of 10-class deep feature representations in a subspace produced by DPQ, GPQ, OPQN-12q, and OPQN. Each color represents a unique identity.

Finally, to intuitively compare the feature representations in a subspace learned by different deep quantization methods, we illustrate visualizations of the sub-vectors under 36-bit codes on the VGGFace2 dataset in Figure 9. Ten identities are randomly selected from the testing set, and the trained deep quantization models are deployed on the samples to generate feature vectors directly.

Instead of using the complete vector for visualization, we visualize sub-vectors, for which the quantization is performed by each codebook individually. In the experiment, the first 512-dimensional features are split from the 2048-dimensional bottleneck features. t-SNE (Maaten and Hinton, 2008) is applied to map the high-dimensional features of each method to 2-dimensions. From Figure 9, OPQN produces the most separable feature representations in the subspace with the least overlapping when compared with the other methods. The visualization results confirm that OPQN has the most discriminative power to learn sub-vectors of feature representations for quantization.

To summarize the three-dataset results under the standard retrieval setting, the superiority of OPQN is due to the following reasons. 1) The concepts of quantization to learning and the orthonormal codewords help enhance informativeness of quantization and reduce redundancy in the codewords. The soft quantization strategy explicitly decorrelates the feature and probability, which provides greater flexibility in the composition of the quantization when codewords are predefined. 2) The network can maximize the discriminability in soft quantizations, and in the original features, by benefiting from the joint subspace-wise classification loss, while the optimization on the original features facilitates obtaining better quantization representations.

Table 2 MAP results on VGGFace2, CFW-60K and YouTube Faces under the unseen identities retrieval setting

Method	VGGFace2				CFW-60K				YouTube Faces			
	24-bit	36-bit	48-bit	64-bit	24-bit	36-bit	48-bit	64-bit	24-bit	36-bit	48-bit	64-bit
DDQH*	0.0771	0.0971	0.1239	0.1469	0.0652	0.0861	0.0987	0.1197	0.0453	0.0685	0.0900	0.1129
DCWH	0.0268	0.0465	0.0648	0.0813	0.0208	0.0359	0.0498	0.0624	0.0271	0.0525	0.0780	0.0963
DPAH	0.0271	0.0499	0.0625	0.1122	0.0255	0.0404	0.0512	0.0868	0.0226	0.0386	0.0572	0.0943
CSQ	0.0230	0.0286	0.0336	0.0382	0.0225	0.0239	0.0309	0.0370	0.0241	0.0275	0.0373	0.0435
DCDH*	0.0315	0.0589	0.0700	0.0905	0.0336	0.0570	0.0621	0.0735	0.0256	0.0433	0.0489	0.0640
DPQ	0.0767	0.0821	0.0899	0.1368	0.0551	0.0622	0.0682	0.1001	0.0520	0.0608	0.0702	0.1075
GPQ	0.1024	0.1069	0.1124	-	0.0852	0.0896	0.0942	-	0.0424	0.0469	0.0503	-
OPQN (Ours)	0.1529	0.2227	0.2593	0.3419	0.1281	0.1808	0.2075	0.2554	0.1044	0.1612	0.2079	0.2659
OPQN-l2q	0.0729	0.1084	0.1550	0.2200	0.0606	0.0877	0.1245	0.1761	0.0621	0.0827	0.1600	0.2333

4.5 Unseen Identities Retrieval

Different from the standard retrieval setting, where the evaluation dataset contains the same set of classes as the training dataset, Klein and Wolf (2019) used a set of unseen classes as queries and the database for unseen classes retrieval. The importance of examining a hashing technique for unseen classes retrieval has been highlighted in Sablayrolles et al (2017), but prior hashing-based face image retrieval works have not provided the results under this setting.

The employed protocol is given as follows. The deep hashing/quantization models have been pre-trained on the VGGFace2 training set under the standard retrieval setting. These models are used for feature extraction and representation of unseen identities' images. We evaluate three different datasets. One is the official testing set of VGGFace2, with its image items further divided into a database-query split as detailed in Sect. 4.1.3. The others are the CFW-60K

and YouTube Faces datasets. We conduct experiments on the database-query splits as described in Sects. 4.1.2 and 4.1.4. In addition to MAP, which measures the overall performance, $P@T$ is used to emphasize the top ranking. Specifically, $P@10$ is used for the VGGFace2, while $P@5$ is used for CFW-60K and YouTube Faces datasets.

The MAP and $P@T$ results of unseen identities retrieval on three datasets are shown in Tables 2 and 3, respectively. From Table 2, OPQN performs the best over all the compared code lengths for unseen identities retrieval. Its MAP performance surpasses the second place GPQ by 10.44% and 8.25% on average, respectively, on VGGFace2 and CFW-60K datasets. On YouTube Faces, it outperforms the second place DDQH* by 10.57% on average. Compared with the variant l2q method, OPQN achieves better generalization ability with an average superiority of 10.51%, 8.07%, and 5.03% on VGGFace2, CFW-60K, and YouTube Faces, respectively. The results confirm

Table 3 P@T results on VGGFace2, CFW-60K and YouTube Faces under the unseen identities retrieval setting

Method	VGGFace2 (P@10)				CFW-60K (P@5)				YouTube Faces (P@5)			
	24-bit	36-bit	48-bit	64-bit	24-bit	36-bit	48-bit	64-bit	24-bit	36-bit	48-bit	64-bit
DDQH*	0.1985	0.2728	0.3391	0.4000	0.1394	0.2014	0.2349	0.2844	0.1177	0.1748	0.2306	0.2805
DCWH	0.1367	0.2313	0.3058	0.3598	0.0846	0.1426	0.2024	0.2435	0.1001	0.1842	0.2577	0.3047
DPAH	0.1221	0.2161	0.2753	0.4038	0.0821	0.1429	0.1758	0.2673	0.0774	0.1343	0.1902	0.2813
CSQ	0.1255	0.1615	0.1803	0.2202	0.0752	0.0914	0.1165	0.1297	0.0848	0.1012	0.1236	0.1491
DCDH*	0.1426	0.2063	0.2915	0.3489	0.1003	0.1583	0.1828	0.2336	0.0853	0.1321	0.1620	0.2042
DPQ	0.2151	0.2621	0.3407	0.4057	0.1492	0.1768	0.1900	0.2677	0.1283	0.1465	0.1600	0.2851
GPQ	0.2051	0.2165	0.2258	-	0.1658	0.1682	0.1724	-	0.0817	0.0919	0.0948	-
OPQN (Ours)	0.3987	0.5131	0.5823	0.6932	0.3050	0.4090	0.4500	0.5628	0.2217	0.3556	0.4577	0.5505
OPQN-l2q	0.2638	0.3664	0.4788	0.5976	0.1894	0.2508	0.3691	0.4750	0.1797	0.2348	0.3519	0.4649

the effectiveness of the proposed orthonormal constraint on codewords to both standard retrieval and unseen identity retrieval, which is crucial to scalable face image retrieval. However, one can observe a dramatic decrease in the performance of all the pre-trained deep quantization/ hashing models compared with that on seen identities retrieval (Table 1), indicating the great difficulty in the task.

As for P@T results in Table 3, the pre-trained OPQN model still generalizes significantly better than other methods with results of nearly 70% P@10 and more than 55% P@5 on the VGGFace2 and other two datasets at 64 bits. And the results are 28.75%, 27.84%, and 24.58% higher than the second best methods DPQ (VGGFace2), DDQH (CFW-60K) and DCWH (YouTube Faces), respectively. The P@T performance of OPQN averaged over all bit values on the VGGFace2, CFW-60K, and YouTube Faces datasets are better than the second best methods

DPQ, DDQH, and DCWH by 24.09%, 21.67% and 18.47%, respectively. Once again, using predefined orthonormal codewords considerably improves the performance of OPQN over OPQN-l2q, inducing an average improvement of 12.02% (VGGFace2), 11.06% (CFW-60K), and 8.86% (YouTube Faces) on three datasets. Since retrieving all the related samples is much more challenging than retrieving the most related samples, one can find the substantial performance gap between MAP and P@T results comparing Tables 2 and 3. Considering the high priority of top returned items in a face image retrieval system, the long-bit P@T results of OPQN are still encouraging.

There are two noteworthy observations from Tables 2 and 3. Firstly, the baseline deep quantization methods, including OPQN-l2q have comparable or better performance than the deep hashing methods, especially on small bits. However, they are inferior to their deep hashing competitors in the task of seen identities retrieval


































Query	Top 5 retrieved images (P@5)					
						OPQN 100%
	✓	✓	✓	✓	✓	
						DCDH 80%
	✓	✓	✓	✓	✗	
						OPQN 80%
	✓	✓	✓	✓	✗	
						DCDH 60%
	✓	✗	✗	✓	✓	
						OPQN 80%
	✓	✓	✓	✗	✓	
						DCDH 60%
	✗	✓	✗	✓	✓	

Fig. 10 Examples of top-5 retrieved images by OPQN and DCDH under the unseen identities retrieval setting. The models are pre-trained with 64-bit codes and evaluated on the VGGFace2 dataset.

(Table 1). The reason is that unlike hashing methods, which cause information loss when transforming real-valued features to binary codes, PQ-based methods use real-valued codewords to reduce the deviations generated during encoding. With the exponential number of combinations on codewords, deep quantization methods also enable more fine-grained and diverse distance measurements between the database and queries. We further visualize the top samples returned by OPQN in comparison with DCDH, which is the second best method for standard retrieval, in Figure 10. It is straightforward to see that our method can return more truly related items when given an unseen identity as the query.

The second observation is that the unseen identities retrieval performance, measured by both MAP and P@T, consistently improved with increasing code length for all methods. We conclude that longer binary code representations effectively improve the generalization ability of deep hashing/quantization methods. Note that it is feasible for OPQN to learn longer than 64-bit codes by enlarging the dimension of the bottleneck features. Thus, the unseen identities retrieval performance could be further enhanced.

5 Discussion

5.1 Ablation Study

We investigate four variants of OPQN that apply different loss function designs.

5.1.1 OPQN-A

In the OPQN-A method, the learning metric only utilizes information within soft representations for training and the discriminability of the original features is discarded. In other words, the classification loss L_{clf} in OPQN-A only contains the part derived in Eq. (7).

5.1.2 OPQN-C

The OPQN-C variant concatenates the composed soft representations and original sub-vectors in all the subspaces to full vectors before being fed into the classifier. OPQN-C considers the ensemble x_i

and s_i with the whole dimension, and the weight matrix of the classifier is also adjusted to the whole dimension. Thus, it only utilizes the visual information of x_i and s_i in the concatenated space.

5.1.3 OPQN-S

The OPQN-S variant replaces the angular margin-based classifier with a traditional softmax classifier as used in DPQ. Thus, no ℓ_2 normalization is applied to sub-vectors, soft representations, or weight vectors. It still utilizes soft quantization and the original feature vectors in each subspace for training.

5.1.4 OPQN-W

The OPQN-W variant represents the finalized objective function without the regularization term L_{ent} shown in Eq. (9). This variant is set to observe to what extent the one-hot encoding of codewords can improve the performance of image retrieval.

For a fair comparison, the same codeword configuration as in the original OPQN are applied to the four variants. These variants, and OPQN, all use predefined orthonormal codewords. We report the MAP results of these variants on FaceScrub and CFW-60K datasets in Table 4. One can see that all these methods exhibit different degrees of deterioration in performance as measured by MAP compared to OPQN. The comparison of OPQN-A and OPQN shows that involving original feature

information in training is beneficial to obtain more discriminative representations. The improvement in performance from OPQN-C to OPQN verifies the advantage of discriminability maximization in each subspace for better precision in quantization. OPQN-S performs the worst among the four variants. As OPQN works with sub-vectors, instead of concatenated full vectors as in DPQ, it indicates the necessity of ℓ_2 normalization and the angular margin for removal of radial variations and learning of separable representations. Finally, from the comparison of OPQN-W and OPQN, the entropy-based regularization boosts the performance under tiny code lengths, e.g., 16-bit, while for longer bits, our OPQN slightly performs better than OPQN-W. Basically, the one-hot encoding prompts smaller quantization errors to represent database items. It means that disturbances from quantization errors may be more severe under short bit lengths. With longer bits, the adverse impact is lessened due to more possible combinations of codewords for quantization.

5.2 Codebook Configuration

We further explore the influence of different codebook configurations on binary code performance. Basically, a l -bit binary code can be generated in the form of $l = M \times O$, where M is the number of codebooks, $O = \log_2 K$, and K is the number of codewords per codebook. Thus, binary codes with the same length can be obtained from different

Table 4 MAP results of three variants of OPQN for seen identities retrieval

Method	FaceScrub				CFW-60K			
	16-bit	24-bit	36-bit	48-bit	16-bit	24-bit	36-bit	48-bit
OPQN-A	0.6059	0.8762	0.8932	0.8989	0.2348	0.7497	0.8052	0.8172
OPQN-C	0.6164	0.8807	0.8390	0.8311	0.5455	0.7847	0.7384	0.7423
OPQN-S	0.2016	0.2892	0.6072	0.7888	0.1686	0.2618	0.6215	0.7281
OPQN-W	0.8066	0.9072	0.9240	0.9336	0.7338	0.8539	0.8789	0.8862
OPQN	0.9032	0.9154	0.9270	0.9385	0.8547	0.8637	0.8826	0.8940

combinations of M and O . For simplicity, we consider two relative configurations with K ranging between 2^6 and 2^9 : the first configuration adopts bigger M and smaller O for encoding while the other uses smaller M and bigger O . Two sets of experiments on 24-bit, 36-bit, and 48-bit codes are conducted w.r.t two configurations. The combinations of the first configuration are 4×6 , 6×6 , and 8×6 for three code lengths, while the other configuration uses 3×8 , 4×9 , 6×8 as code lengths.

The standard retrieval results on FaceScrub and VGGFace2 under different codebook configurations are presented in Table 5. We can see performance improvement in almost all the cases when using a larger O for quantization. These improvements are more distinct for the VGGFace2 dataset. OPQN performs better with a larger value of K , especially for smaller bits. Using more codewords in a codebook implies richer prototypes in the subspace for quantization, making it easier for sub-vectors to find the nearest prototype with less quantization error. By using $K = 256$, rather than $K = 64$, under 24-bit codes on the VGGFace2 dataset, OPQN can achieve nearly a

90% MAP score and the performance of 36-bit codes with a 4×9 configuration is better than that with 48-bit codes. The benefit of a larger K may become less with longer bit codes as the increase in the number of subspaces might reduce the quantization burden and so mitigate the benefit of a larger value of K .

Table 5 Comparison of MAP results by different codebook configurations

Dataset	24-bit		36-bit		48-bit	
	4×6	3×8	6×6	4×9	8×6	6×8
FaceScrub	0.9154	0.9298	0.9270	0.9367	0.9385	0.9329
VGGFace2	0.7722	0.8986	0.9026	0.9508	0.9386	0.9504

5.3 Parameter Sensitivity

The effect of parameters on model performance is examined. From the ablation study shown in Table 4, entropy-based regularization mainly exhibits its advantage under short codes. Thus, we present MAP results w.r.t. different values

Table 6 16-bit MAP results w.r.t. different values of λ

λ	0	0.01	0.05	0.1	0.3
FaceScrub	0.8066	0.8247	0.8543	0.9032	0.0159
CFW-60K	0.7338	0.7628	0.7801	0.8547	0.1029

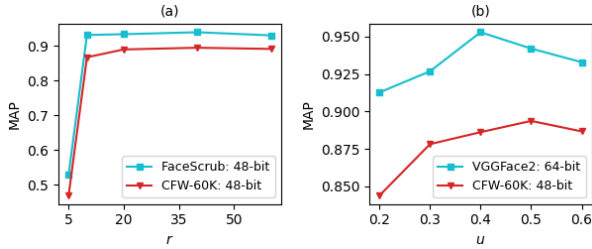


Fig. 11 (a) MAP results w.r.t. different values of the scaling factor r under the two experimental settings, (b) MAP results w.r.t. different values of the margin u under the two experimental settings.

of the balance weight, λ under 16-bit codes in Table 6. One can see that the performance increases steadily as the regularization with λ varies from 0.01 to 0.1 but decreases sharply for values bigger than 0.1.

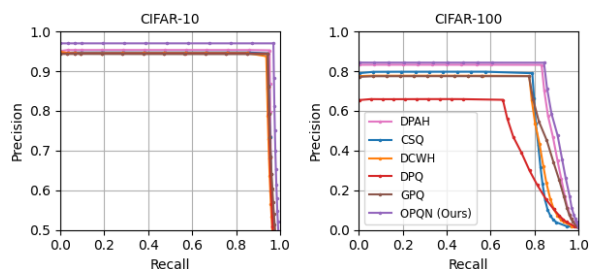
We then study the impacts of the scaling factor r and the angular margin u , in Eqs. (6) and (7). The plots of MAP performances w.r.t. different values of r and u are illustrated in Figures 11(a) and 11(b), respectively. From Figure 11(a), performance measured by MAP improves substantially from $r = 5$ to $r = 10$, reaching good values, and then is nearly stable. In Figure 11(b), as u increases from 0.2 to 0.6, the performance of the model rises and then decreases. The inflection point appears earlier on the VGGFace2 dataset with the best values of u being around 0.4 in VGGFace2 and 0.5 in CFW-60K dataset. Generally, the model performs robustly under variations of u .

5.4 Extension Experiments on General Image Datasets

One may wonder how the proposed OPQN performs for the general image retrieval task. Therefore, this paper further conducts experiments comparing other state-of-the-art methods on two benchmark CIFAR (Krizhevsky et al, 2009) datasets: CIFAR-10 and CIFAR-100. **CIFAR-10** consists of 10 categories containing 60,000 images. The dataset is officially split into 50,000 images for training with 5,000 images per category and 10,000 images for testing with 1,000 images per category. Similar to CIFAR-10, **CIFAR-100** is a dataset with more fine-grained classes, which contains 100 categories with 600 images per class. The images from each class in CIFAR-100 are divided into 500 images for training and 100 images for testing. Following the setup in Zhe et al (2020); Li et al (2020); Zhang and Yan (2021), we use the official testing splits of two datasets as the query set, and the remaining images are used as database images. The training is conducted on all the database images. For simplicity, we unify the backbone network for all the compared methods to be the off-the-shelf ResNet50 (He et al, 2016), pre-trained on ImageNet. Thus, some methods have better MAP performance than presented in their original papers where a shallow backbone network is applied.

Table 7 MAP results on CIFAR-10 and CIFAR-100 for standard retrieval

Method	CIFAR-10			CIFAR-100		
	16-bit	32-bit	64-bit	16-bit	32-bit	64-bit
DSDH	0.944	0.946	0.944	0.102	0.179	0.213
CSQ	0.957	0.961	0.959	0.775	0.802	0.805
DPAH	0.959	0.964	0.969	0.817	0.844	0.857
DCWH	0.956	0.960	0.957	0.734	0.768	0.807
DPQ	0.952	0.954	0.953	0.722	0.739	0.706
GPQ	0.954	0.955	0.957	0.802	0.814	0.817
OPQN	0.966	0.972	0.978	0.863	0.868	0.873

**Fig. 12** PR curve performance on the CIFAR-10 and CIFAR-100 under 64-bit codes.

We compare with a series of popular deep hashing/quantization methods specified for general image retrieval tasks, including DSDH (Li et al, 2020), DCWH (Zhe et al, 2020), DPAH (Wang et al, 2020), CSQ (Yuan et al, 2020), DPQ (Klein and Wolf, 2019), and GPQ (Jang and Cho, 2020). For all the quantization based methods, i.e., DPQ, GPQ, and OPQN, the experiment configurations are set as follows: we fix the number of codewords per codebook to 256, and the number of codebooks are 2, 4, 8 for 16, 32 and 64-bit codes, respectively.

The results of MAP performance on CIFAR-10 and CIFAR-100 are shown in Table. 7. We can see that the proposed OPQN consistently outperforms all the compared methods over the three

code lengths on the two datasets. On CIFAR-10, OPQN surpasses the second place DPAH by 0.80% on average. The superiority of OPQN is more prominent to exhibit on the CIFAR-100 with more classes. Specifically, it defeats the second place DPAH by 2.87% on average. For the short code length of 16-bit, OPQN is the only method that achieves higher than 85% MAP, outperforming DPAH with a distinct margin of 4.60%. Figure. 12 illustrates the PR-curve performances of 64-bit codes on the CIFAR-10 and CIFAR-100 datasets, respectively. In summary, the superiority of OPQN over state-of-the-art quantization/hashing methods is not limited to face image retrieval task but extended to general image retrieval. This confirms the effectiveness of the proposed scheme’s predefined orthonormal codewords and the discriminative power of the carefully designed subspace-wise joint classification loss.

6 Conclusion

This paper develops a deep product quantization-based method, OPQN, particularly for face image retrieval. Unlike previous deep quantization works, a novel framework is proposed using predefined orthonormal codewords for quantization. We design a tailored loss function as the learning metric to maximize discriminability in both the soft quantization and original features in all subspaces. Extensive experiments are conducted

on several widely-employed face image datasets where OPQN is compared with a series of deep hashing/quantization methods. The results show that OPQN outperforms the other methods under both seen and unseen identities retrieval settings. The other deep quantization methods could obtain competitive generalization performance compared with their deep hashing competitors, even if their results for seen identities retrieval are inferior. This suggests an inherent advantage of product quantization over binary hashing for unseen identities retrieval. Furthermore, the proposed orthonormal codewords consistently boost both the standard retrieval performance and model generalization ability, verifying the importance of codewords distribution to quantization quality. From the experiments extended to general image datasets, OPQN can still achieve satisfactory results, providing a general solution for deep quantization-based image retrieval tasks.

Future work could include investigating how the complete visual information is scattered into subspaces in the quantization method. The sub-vector of bottleneck features in different subspaces may describe specific facial regions or attributes. Thus, the designed subspace-wise learning metric presented here should be adaptable to different parts of visual discriminability. This would enable automatic choice of optimal values of the margin u and the scaling factor r .

Acknowledgments

This work is supported by Hong Kong Innovation and Technology Commission (InnoHK Project CIMDA), Hong Kong Research Grants Council (Project 11204821), and City University of Hong Kong (Project 9610034).

References

- Ahmed N, Natarajan T, Rao KR (1974) Discrete cosine transform. *IEEE transactions on Computers* 100(1):90–93
- Babenko A, Lempitsky V (2014) Additive quantization for extreme vector compression. In: *CVPR*, pp 931–938
- Cao Q, Shen L, Xie W, et al (2018) Vggface2: A dataset for recognising faces across pose and age. In: *FG, IEEE*, pp 67–74
- Cao Y, Long M, Wang J, et al (2016) Deep quantization network for efficient image retrieval. In: *Proceedings of the AAAI Conference on Artificial Intelligence*
- Deng J, Guo J, Xue N, et al (2019) Arcface: Additive angular margin loss for deep face recognition. In: *CVPR*, pp 4690–4699
- Ge T, He K, Ke Q, et al (2013) Optimized product quantization for approximate nearest neighbor search. In: *CVPR*, pp 2946–2953

- Gong Y, Lazebnik S, Gordo A, et al (2012) Iterative quantization: A procrustean approach to learning binary codes for large-scale image retrieval. *IEEE transactions on pattern analysis and machine intelligence* 35(12):2916–2929
- Gui J, Liu T, Sun Z, et al (2017) Fast supervised discrete hashing. *IEEE transactions on pattern analysis and machine intelligence* 40(2):490–496
- Hartigan JA, Wong MA (1979) Algorithm as 136: A k-means clustering algorithm. *Journal of the royal statistical society series c (applied statistics)* 28(1):100–108
- He K, Zhang X, Ren S, et al (2016) Deep residual learning for image recognition. In: *CVPR*, pp 770–778
- Ioffe S, Szegedy C (2015) Batch normalization: accelerating deep network training by reducing internal covariate shift. In: *International Conference on Machine Learning (ICML)*, pp 448–456
- Jang YK, Cho NI (2020) Generalized product quantization network for semi-supervised image retrieval. In: *CVPR*, pp 3420–3429
- Jegou H, Douze M, Schmid C (2010) Product quantization for nearest neighbor search. *IEEE transactions on pattern analysis and machine intelligence* 33(1):117–128
- Klein B, Wolf L (2019) End-to-end supervised product quantization for image search and retrieval. In: *CVPR*, pp 5041–5050
- Krizhevsky A, Hinton G, et al (2009) Learning multiple layers of features from tiny images
- Li Q, Sun Z, He R, et al (2017) Deep supervised discrete hashing. In: *NIPS*, pp 2482–2491
- Li Q, Sun Z, He R, et al (2020) A general framework for deep supervised discrete hashing. *International Journal of Computer Vision* 128(8):2204–2222
- Li WJ, Wang S, Kang WC (2016) Feature learning based deep supervised hashing with pairwise labels. In: *IJCAI*, pp 1711–1717
- Li Y, Wang R, Liu H, et al (2015) Two birds, one stone: Jointly learning binary code for large-scale face image retrieval and attributes prediction. In: *ICCV*, pp 3819–3827
- Lin J, Li Z, Tang J (2017) Discriminative deep hashing for scalable face image retrieval. In: *IJCAI*, pp 2266–2272
- Liu B, Cao Y, Long M, et al (2018) Deep triplet quantization. In: *Proceedings of the 26th ACM international conference on Multimedia*, pp 755–763
- Liu W, Wen Y, Yu Z, et al (2017) SpheroFace: Deep hypersphere embedding for face recognition. In:

- CVPR, pp 212–220
- Maaten Lvd, Hinton G (2008) Visualizing data using t-sne. *Journal of machine learning research* 9(Nov):2579–2605
- Ng HW, Winkler S (2014) A data-driven approach to cleaning large face datasets. In: *ICIP, IEEE*, pp 343–347
- Paszke A, Gross S, Massa F, et al (2019) Pytorch: An imperative style, high-performance deep learning library. *Advances in neural information processing systems* 32:8026–8037
- Sablayrolles A, Douze M, Usunier N, et al (2017) How should we evaluate supervised hashing? In: *2017 IEEE International Conference on Acoustics, Speech and Signal Processing (ICASSP)*, IEEE, pp 1732–1736
- Shen F, Shen C, Liu W, et al (2015) Supervised discrete hashing. In: *CVPR*, pp 37–45
- Shi X, Guo Z, Xing F, et al (2020) Anchor-based self-ensembling for semi-supervised deep pairwise hashing. *International Journal of Computer Vision* 128:2307–2324
- Srivastava N, Hinton G, Krizhevsky A, et al (2014) Dropout: a simple way to prevent neural networks from overfitting. *Journal of Machine Learning Research* 15(1):1929–1958
- Tang J, Lin J, Li Z, et al (2018) Discriminative deep quantization hashing for face image retrieval. *IEEE transactions on neural networks and learning systems* 29(12):6154–6162
- Wang H, Wang Y, Zhou Z, et al (2018) Cos-face: Large margin cosine loss for deep face recognition. In: *CVPR*, pp 5265–5274
- Wang R, Wang R, Qiao S, et al (2020) Deep position-aware hashing for semantic continuous image retrieval. In: *Proceedings of the IEEE/CVF Winter Conference on Applications of Computer Vision*, pp 2493–2502
- Wang X, Shi Y, Kitani KM (2016a) Deep supervised hashing with triplet labels. In: *ACCV*, Springer, pp 70–84
- Wang X, Zhang T, Qi GJ, et al (2016b) Supervised quantization for similarity search. In: *CVPR*, pp 2018–2026
- Weiss Y, Torralba A, Fergus R (2009) Spectral hashing. In: *Advances in neural information processing systems*, pp 1753–1760
- Wolf L, Hassner T, Maoz I (2011) Face recognition in unconstrained videos with matched background similarity. In: *CVPR*, pp 529–534
- Xiong Z, Wu D, Gu W, et al (2020) Deep discrete attention guided hashing for face image

- retrieval. In: Proceedings of the 2020 International Conference on Multimedia Retrieval, pp 136–144
- Yao T, Long F, Mei T, et al (2016) Deep semantic-preserving and ranking-based hashing for image retrieval. In: IJCAI, pp 3931–3937
- Yu T, Yuan J, Fang C, et al (2018) Product quantization network for fast image retrieval. In: Proceedings of the European Conference on Computer Vision (ECCV), pp 186–201
- Yu T, Meng J, Fang C, et al (2020) Product quantization network for fast visual search. International Journal of Computer Vision 128(8):2325–2343
- Yuan L, Wang T, Zhang X, et al (2020) Central similarity quantization for efficient image and video retrieval. In: CVPR, pp 3083–3092
- Zhang K, Zhang Z, Li Z, et al (2016) Joint face detection and alignment using multitask cascaded convolutional networks. IEEE Signal Processing Letters 23(10):1499–1503
- Zhang M, Yan H (2021) Improved deep class-wise hashing with centers similarity learning for image retrieval. In: 2020 25th International Conference on Pattern Recognition (ICPR), IEEE, pp 10,516–10,523
- Zhang M, Zhe X, Chen S, et al (2021) Deep center-based dual-constrained hashing for discriminative face image retrieval. Pattern Recognition p 107976
- Zhang T, Du C, Wang J (2014) Composite quantization for approximate nearest neighbor search. In: International Conference on Machine Learning, PMLR, pp 838–846
- Zhe X, Chen S, Yan H (2020) Deep class-wise hashing: Semantics-preserving hashing via class-wise loss. IEEE transactions on neural networks and learning systems 31(5):1681–1695